INTERNATIONAL JOURNAL FOR NUMERICAL METHODS IN ENGINEERING
Int. J. Numer. Meth. Engng 2003; **56**:2199–2211 (DOI: 10.1002/nme.660)

Failure analysis of solder joints with a damage-coupled viscoplastic model

Y. Wei[1], C. L. Chow[1,*,†], M. K. Neilsen[2] and H. E. Fang[2]

[1]*Department of Mechanical Engineering, University of Michigan-Dearborn, Dearborn, MI 48128, U.S.A.*
[2]*Sandia National Laboratories, Albuquerque, NM 87185, U.S.A.*

SUMMARY

This paper presents failure analysis of solder joints with a damage-coupled viscoplastic model. A material model is developed to characterize the elasticity, plasticity, creep and damage of solder. A semi-implicit time-integration approach is adopted for the numerical implementation of the solder model. This solder model has been implemented into finite element codes developed at Sandia National Laboratories and into the commercial, finite element code ABAQUS^{TM} with its user-defined material subroutine UMAT. Finite element analyses are performed on solder joints with the new solder constitutive model and mesh dependency of these analyses is investigated. Copyright © 2003 John Wiley & Sons, Ltd.

KEY WORDS: damage; viscoplasticity; solder joint; finite element algorithm

1. INTRODUCTION

In the finite element failure analysis of solder joints, two problems need to be addressed: one relates to local material behaviour at the constitutive level and another, global equilibrium of a solder joint. At the local level, a comprehensive constitutive model is required to characterize the complex behaviour of solder under thermo-mechanical loads [1–5]. The development of this constitutive model is difficult due to the combination of elasticity, plasticity, creep, damage and micro-structural evolution that must be captured. Numerical implementation of the model is also difficult due to the stiffness of the governing differential equations. Several numerical algorithms have been reported in the past for complex constitutive models on the subjects of efficiency, non-linear instability and mesh dependence [6–9].

*Correspondence to: C. L. Chow, Department of Mechanical Engineering, University of Michigan-Dearborn, 4901 Evergreen Road, Dearborn, Michigan 48128, U.S.A.
†E-mail: clchow@.umich.edu

Contract/grant sponsor: United States Department of Energy; contract/grant number: DE-ACO4-94AL85000

Received 17 September 2001
Revised 15 March 2002
Accepted 10 June 2002

In this paper, failure analyses of solder joints is carried out with a damage-coupled constitutive model. The model has been successfully applied to many aspects of the thermo mechanical behaviour for 63Sn–37Pb solder bulk material, taking into account the effects of temperature and rate dependence, damage and grain coarsening and isothermal fatigue loading [5, 10, 11]. The numerical simulation in this study is achieved by developing a semi-implicit time-integration approach at the constitutive level. The approach employs an implicit integration procedure for incremental inelastic strain, but an explicit procedure for other internal state variables [12]. To achieve the global equilibrium, a damaged-coupled instantaneous tangent stiffness (Jacobian) matrix is derived. The model has been implemented into finite element codes developed at Sandia National Laboratories and the commercial finite element code ABAQUS^{TM} (version 6.2) through its user-defined subroutine UMAT. Experimental tests and numerical simulations of solder joints made of 63Sn–37Pb alloy are carried out under monotonic tensile loading. In addition to the stress and strain distributions, the damage-coupled model is also able to predict the damage distribution in a joint structure. The distribution enables the identification of a failure site when the calculated damage accumulation reaches a critical value for the material.

2. DAMAGE-COUPLED CONSTITUTIVE EQUATIONS

A damage-coupled viscoplastic model for solder has been developed with the concept of damage mechanics [5, 11]. Two damage variables D and μ are introduced to quantify the damage accumulation in the solder material. For the phase coarsening behaviour of the solder material, a scalar state variable λ is proposed to represent the mean Pb-rich particle diameter. The total strain rate $\dot{\boldsymbol{\varepsilon}}$ is assumed to be the sum of the elastic strain rate $\dot{\boldsymbol{\varepsilon}}^{e}$ and the inelastic strain rate $\dot{\boldsymbol{\varepsilon}}^{in}$

$$\dot{\boldsymbol{\varepsilon}} = \dot{\boldsymbol{\varepsilon}}^{e} + \dot{\boldsymbol{\varepsilon}}^{in} \tag{1}$$

The damage-coupled elastic equation has the form

$$\boldsymbol{\varepsilon}^{e} = \mathbf{C}^{-1} : \boldsymbol{\sigma} \tag{2}$$

where $\boldsymbol{\varepsilon}^{e}$ is the elastic strain tensor, $\boldsymbol{\sigma}$ is the Cauchy stress tensor and $\mathbf{C}$ is the effective isotropic, elastic tensor taking into account the effects of damage for a damaged material. The 6×6 matrix form of the effective elastic tensor is formulated as

$$\mathbf{C}^{-1} = \frac{1}{E}\begin{bmatrix} 1 & -v & -v & 0 & 0 & 0 \\ -v & 1 & -v & 0 & 0 & 0 \\ -v & -v & 1 & 0 & 0 & 0 \\ 0 & 0 & 0 & 2(1+v) & 0 & 0 \\ 0 & 0 & 0 & 0 & 2(1+v) & 0 \\ 0 & 0 & 0 & 0 & 0 & 2(1+v) \end{bmatrix} \tag{3}$$

$$E = \frac{E_0(1-D)^2}{1-4v_0\mu+2(1-v_0)\mu^2}$$

$$v = \frac{v_0 - 2(1-v_0)\mu - (1-3v_0)\mu^2}{1-4v_0\mu+2(1-v_0)\mu^2} \tag{4}$$

E_0 and v_0 are Young's modulus and Poisson's ratio for as-fabricated material, E and v are the effective Young's modulus and the effective Poisson's ratio for damaged material under load, and D and μ are damage variables.

The inelastic strain rate is formulated as

$$\dot{\boldsymbol{\varepsilon}}^{\text{in}} = \dot{p}^{\text{in}} \frac{3}{2} \frac{\mathbf{S}-\mathbf{X}}{J_2} \tag{5}$$

where J_2 is a second invariant of stress difference defined as

$$J_2 = \{\tfrac{3}{2}(\mathbf{S}-\mathbf{X}) : (\mathbf{S}-\mathbf{X})\}^{1/2} \tag{6}$$

$\mathbf{S}$ is the deviatoric stress tensor, $\mathbf{X}$ is the deviatoric back stress tensor and $\dot{p}^{\text{in}}$ is the equivalent inelastic strain rate. The equivalent inelastic strain rate $\dot{p}^{\text{in}}$ is expressed with the effects of damage and coarsening as [3, 5, 11]

$$\dot{p}^{\text{in}} = \frac{1-\mu}{1-D} f \exp\left(\frac{-Q}{RT}\right) \left(\frac{\lambda_0}{\lambda}\right)^p \sinh^m \left(\frac{1-\mu}{1-D} \frac{J_2}{c+\hat{c}}\right) \tag{7}$$

where f, p, m and Q are material parameters, R is the gas constant, T is the absolute temperature, λ is the current mean diameter of the Pb-rich phase, λ_0 is the initial phase diameter, and c and $\hat{c}$ are state variables.

The damage-coupled kinematic hardening equation is

$$\boldsymbol{\alpha}_k = \frac{3}{2} \frac{(1-\mu)^2}{(1-D)^2 C_{k0}} \mathbf{X} \tag{8}$$

where $\boldsymbol{\alpha}_k$ is the back strain tensor and C_{k0} is the parameter for kinematic hardening. Evolution of the scalar state variable c is given as

$$\dot{c} = A_1 \dot{p}^{\text{in}} - (A_2 \dot{p}^{\text{in}} + A_3)(c - c_0)^2 \tag{9}$$

The back strain tensor has the form

$$\dot{\boldsymbol{\alpha}}_k = \dot{\boldsymbol{\varepsilon}}^{\text{in}} - C_{k0}(A_4 \dot{p}^{\text{in}} + A_5)\boldsymbol{\alpha}_k \sqrt{\tfrac{2}{3}\boldsymbol{\alpha}_k : \boldsymbol{\alpha}_k} \tag{10}$$

The state variable $\hat{c}$ is related to the phase size λ by

$$\hat{c} = A_6 \left(\frac{\lambda_0}{\lambda}\right)^{A_7} \tag{11}$$

Evolution of the phase size for 63Sn–37Pb is given by experiments [13]

$$\dot{\lambda} = \frac{1.05 \times 10^{-5} \mathrm{e}^{-11023/T} + 4.00 \times 10^{-8} \mathrm{e}^{-3123/T} \dot{p}^{\text{in}}}{(\lambda - \lambda_0)^{2.9}} \tag{12}$$

where $c_0, A_1, A_2, A_3, A_4, A_5, A_6$ and A_7 are material parameters.

The damage accumulation is dependent upon loading path. For monotonic loading, the damage accumulates rapidly. However, the damage rate becomes slow under strain-controlled cyclic loading. In order to characterize the type of damage accumulation, the concept of a damage surface in strain space is proposed. The damage surface bounds the regime of fatigue damage. This is analogous to a yield surface in plasticity theory which bounds the regime of elastic behaviour. When the damage state in a material is located within the damage surface, fatigue damage accumulates. When the state is on the damage surface expanding outwards, inelastic damage generates. In general, the inelastic damage rate is much faster than the fatigue damage rate. For the damage hardening material, the damage surface expands as inelastic damage accumulates. In this investigation, the damage surface can be mathematically described in strain space as

$$F_{\mathrm{d}} = p^{\mathrm{in}} - p^{\mathrm{in}}_{\max} = 0 \tag{13}$$

where p^{in} is a scalar measure of the inelastic strain, and $p^{\mathrm{in}}_{\max}$ is the maximum value that this scalar measure has obtained during previous loading. The scalar measure of inelastic strain, p^{in}, is defined as

$$p^{\mathrm{in}} = \sqrt{\tfrac{2}{3}\,\boldsymbol{\varepsilon}^{\mathrm{in}} : \boldsymbol{\varepsilon}^{\mathrm{in}}} \tag{14}$$

where $\boldsymbol{\varepsilon}^{\mathrm{in}}$ is the inelastic strain tensor. The damage surface described by Equation (13) enlarges when $p^{\mathrm{in}}_{\max}$ increases. Accordingly, the equivalent damage evolution equation is established as:

$$\dot{w} = \begin{cases} \dot{p}^{\mathrm{in}} \left(\dfrac{Y_{\mathrm{d}}}{Y_{\mathrm{h}}} \right)^{B_1} & \text{if } F_{\mathrm{d}} = 0 \quad \text{and} \quad \dfrac{\partial F_{\mathrm{d}}}{\partial \boldsymbol{\varepsilon}^{\mathrm{in}}} : \dot{\boldsymbol{\varepsilon}}^{\mathrm{in}} > 0 \\ \dot{p}^{\mathrm{in}} \dfrac{Y_{\mathrm{d}}}{Y_{\mathrm{hf}}} & \text{if } F_{\mathrm{d}} < 0 \quad \text{or} \quad F_{\mathrm{d}} = 0 \quad \text{and} \quad \dfrac{\partial F_{\mathrm{d}}}{\partial \boldsymbol{\varepsilon}^{\mathrm{in}}} : \dot{\boldsymbol{\varepsilon}}^{\mathrm{in}} \leqslant 0 \end{cases} \tag{15}$$

Evolution equations for damage variables D and μ are expressed as

$$\begin{aligned} \dot{D} &= -\dot{w}\,\frac{Y_D}{2Y_{\mathrm{d}}} \\ \dot{\mu} &= -\dot{w}\,\frac{\gamma Y_\mu}{2Y_d} \end{aligned} \tag{16}$$

where w is the equivalent damage variable, and Y_{d} is the equivalent damage energy release rate as

$$Y_{\mathrm{d}} = [\tfrac{1}{2}(Y_D^2 + \gamma Y_\mu^2)]^{1/2} \tag{17}$$

Y_D and Y_μ are the damage energy release rates corresponding to the damage variables D and μ

$$Y_D = -\frac{1}{1-D}\,\boldsymbol{\sigma} : \mathbf{C}^{-1} : \boldsymbol{\sigma} - \frac{3}{2}\,\frac{(1-\mu)^2}{(1-D)^3 C_{k0}}\,\mathbf{X} : \mathbf{X} \tag{18}$$

$$Y_\mu = -\frac{1}{1-D}\,\boldsymbol{\sigma} : \mathbf{Z} : \boldsymbol{\sigma} + \frac{3}{2}\,\frac{(1-\mu)}{(1-D)^2 C_{k0}}\,\mathbf{X} : \mathbf{X} \tag{19}$$

Table I. 63Sn–37Pb solder material parameters (temperature independent).

Poisson's ratio	0.4
Young's modulus (GPa)	33.26
A_1 (MPa)	0.00E + 00
A_2 (1/MPa)	0.00E + 00
A_3 (1/MPa s)	0.00E + 00
A_6 (MPa)	5.66
A_7	0.5
Flow rate f (1/s)	1.802E + 06
Sinh exponent m	3.04
Growth exponent p	3.00
Flow stress C_0 (MPa)	2.83
Phase size λ_0 (mm)	2.257E − 03
Activation energy Q (cal/mol)	1.376E + 4
Gas constant R (cal/mol K)	1.987
Damage constant B_1	0.4
Damage constant B_2	5.0
Damage constant B_3 (K)	3.34E + 03
Damage constant γ	−0.2
Damage constant Y_0 (MPa)	6.0E − 08

$$\mathbf{Z} = \frac{1}{E_0(1-D)} \begin{bmatrix} z_1 & z_2 & z_2 & 0 & 0 & 0 \\ z_2 & z_1 & z_2 & 0 & 0 & 0 \\ z_2 & z_2 & z_1 & 0 & 0 & 0 \\ 0 & 0 & 0 & 2(z_1 - z_2) & 0 & 0 \\ 0 & 0 & 0 & 0 & 2(z_1 - z_2) & 0 \\ 0 & 0 & 0 & 0 & 0 & 2(z_1 - z_2) \end{bmatrix} \tag{20}$$

$$z_1 = 2\mu(1 - v_0) - 2v_0, \quad z_2 = (1 + \mu)(1 - v_0) - 2\mu v_0$$

Y_h in Equation (15) is the inelastic damage hardening/softening variable and Y_{hf} is the fatigue damage hardening/softening variable. For the 63Sn–37Pb solder alloy, the inelastic damage hardening/softening variable is established from test results:

$$Y_h = Y_0 e^{B_2 w + B_3/T} \tag{21}$$

where γ, Y_0, B_1, B_2 and B_3 are damage-related material constants.

Several uniaxial tests under different loading conditions, i.e. monotonic tension, tensile creep and strain-controlled fatigue, were carried out to determine the material constants for the 63Sn–37Pb solder material. In order to determine damage-related parameters, the effective Young's modulus and Poisson's ratio were measured at certain strain intervals. The material parameters determined for the 63Sn–37Pb solder material are summarized in Tables I and II [5].

Table II. 63Sn–37Pb solder material parameters (temperature dependent).

Temperature (°C)	25	75	100
Temperature (K)	298	348	373
C_{k0} (GPa)	28.15	22.08	19.32
A_4 (1/MPa)	44.95	103.0	153.7
A_5 (1/MPa s)	8.42E − 03	5.95E − 02	0.2

3. FINITE ELEMENT FORMULATION

The proposed model has been implemented into finite element codes developed at Sandia National Laboratories and the commercial finite element code ABAQUS^{TM} (version 6.2) through its user-defined subroutine UMAT. A displacement finite element method is usually applied by the principle of virtual work [14]. It is based on approximating the equilibrium requirement by replacing it with a weaker requirement, that equilibrium must be maintained in an average sense over a finite number of divisions of the volume of the body. A user subroutine UMAT is used to define a material mechanical behaviour in ABAQUS^{TM}. The stresses and solution-dependent state variables are integrated and updated following their evolution equations. The material Jacobian matrix $\partial\Delta\boldsymbol{\sigma}/\partial\Delta\boldsymbol{\varepsilon}$ is provided to search for incremental deformation in order to satisfy the momentum balance equation. In this section, we present discrete constitutive equations and the tangent stiffness matrix.

A semi-implicit time integration is adopted at the constitutive level. From the equivalent inelastic strain rate in Equation (7), we have

$$\frac{\Delta p^{\text{in}}}{\Delta t} = F(\mathbf{S}, \mathbf{X}, \lambda, c, D, \mu) = \frac{1-\mu}{1-D} f \exp\left(\frac{-Q}{RT}\right) \left(\frac{\lambda_0}{\lambda}\right)^p \sinh^{\text{in}}\left(\frac{1-\mu}{1-D}\frac{J_2}{c+\hat{c}}\right) \tag{22}$$

where t is time. The above equation can be re-written as

$$G = \Delta p^{\text{in}} - F\Delta t = 0 \tag{23}$$

This non-linear equation can be solved for Δp^{in} by Newton–Raphson method

$$\Delta p^{\text{in},i+1} = \Delta p^{\text{in},i} - \frac{G(\Delta p^{\text{in},i})}{G'(\Delta p^{\text{in},i})} \tag{24}$$

where $\Delta p^{\text{in},i+1}$ is the increment of the equivalent inelastic strain for the $(i+1)$th iteration, $\Delta p^{\text{in},i}$ is the increment for the ith iteration, the form of $G'(\Delta p^{\text{in}})$ can be derived with Equation (23) as

$$G' = \frac{\mathrm{d}G}{\mathrm{d}(\Delta p^{\text{in}})} = 1 - \frac{\mathrm{d}F}{\mathrm{d}(\Delta p^{\text{in}})}\Delta t = 1 - \left\{ \frac{\partial F}{\partial \mathbf{S}} : \frac{\partial(\Delta \mathbf{S})}{\partial(\Delta p^{\text{in}})} + \frac{\partial F}{\partial \mathbf{X}} : \frac{\partial(\Delta \mathbf{X})}{\partial(\Delta p^{\text{in}})} + \frac{\partial F}{\partial \lambda}\frac{\partial(\Delta\lambda)}{\partial(\Delta p^{\text{in}})} + \frac{\partial F}{\partial c}\frac{\partial(\Delta c)}{\partial(\Delta p^{\text{in}})} + \frac{\partial F}{\partial D}\frac{\partial(\Delta D)}{\partial(\Delta p^{\text{in}})} + \frac{\partial F}{\partial \mu}\frac{\partial(\Delta\mu)}{\partial(\Delta p^{\text{in}})} \right\} \Delta t \tag{25}$$

The iteration process is terminated for the solution of Δp^{in} when the following condition of convergence is satisfied:

$$\left| \frac{\Delta p^{\text{in},i+1} - \Delta p^{\text{in},i}}{\Delta p^{\text{in},i}} \right| \leqslant \text{tolerance (i.e. } 10^{-4}) \tag{26}$$

Other internal state variables are updated at each iteration stepwise by the explicit forward Euler approach with Equations (2), (8)–(12) when $\Delta p^{\text{in},i}$ is determined.

For the semi-implicit time-integration approach described above, the time increment of the global step is limited by the explicit expressions of some internal state variables although larger increment of Δp^{in} can be chosen for integration by means of the implicit backward Euler scheme. Therefore, a sub-incrementation of global time step is introduced for computer efficiency. The time increment of the sub-step is equal to the global time step subdivided by a user-defined sub-step number.

At global equilibrium of the finite element analysis, a damage-coupled instantaneous tangent stiffness (Jacobian) matrix is required. An approximate form is derived from Equation (2) by ignoring the terms associated with the damage rate

$$\Delta\boldsymbol{\sigma} = \mathbf{C} : (\Delta\boldsymbol{\varepsilon} - \Delta\boldsymbol{\varepsilon}^{\text{in}}) = \mathbf{C} : \left(\Delta\boldsymbol{\varepsilon} - \frac{3}{2} \frac{\mathbf{S} - \mathbf{X}}{J_2} \Delta p^{\text{in}} \right) \tag{27}$$

Therefore, the Jacobian matrix is defined as

$$\mathbf{J} = \frac{\partial(\Delta\boldsymbol{\sigma})}{\partial(\Delta\boldsymbol{\varepsilon})} = \mathbf{C} - \frac{3}{2} \left(\mathbf{C} : \frac{\mathbf{S} - \mathbf{X}}{J_2} \right) \otimes \frac{\partial(\Delta p^{\text{in}})}{\partial(\Delta\boldsymbol{\varepsilon})} \tag{28}$$

The expression of $\partial(\Delta p^{\text{in}})/\partial(\Delta\boldsymbol{\varepsilon})$ must be determined to form the Jacobian matrix defined above. From Equation (23), we have

$$\begin{aligned} \frac{\partial(\Delta p^{\text{in}})}{\partial(\Delta\boldsymbol{\varepsilon})} = \frac{\partial F}{\partial(\Delta\boldsymbol{\varepsilon})} \Delta t = \Bigg\{ & \frac{\partial F}{\partial \mathbf{S}} : \frac{\partial(\Delta\mathbf{S})}{\partial(\Delta\boldsymbol{\varepsilon})} + \frac{\partial F}{\partial \mathbf{X}} : \frac{\partial(\Delta\mathbf{X})}{\partial(\Delta\boldsymbol{\varepsilon})} + \frac{\partial F}{\partial \lambda} \frac{\partial(\Delta\lambda)}{\partial(\Delta\boldsymbol{\varepsilon})} \\ & + \frac{\partial F}{\partial c} \frac{\partial(\Delta c)}{\partial(\Delta\boldsymbol{\varepsilon})} + \frac{\partial F}{\partial D} \frac{\partial(\Delta D)}{\partial(\Delta\boldsymbol{\varepsilon})} + \frac{\partial F}{\partial \mu} \frac{\partial(\Delta\mu)}{\partial(\Delta\boldsymbol{\varepsilon})} \Bigg\} \Delta t \end{aligned} \tag{29}$$

The increment of deviatoric stress tensor can be written as

$$\Delta\mathbf{S} = 2G \left(\Delta\boldsymbol{\varepsilon}' - \frac{3}{2} \frac{\mathbf{S} - \mathbf{X}}{J_2} \Delta p^{\text{in}} \right) \tag{30}$$

where G is the effective shear modulus for the damaged material and $\Delta\varepsilon'$ is the deviatoric strain increment. Then we have

$$\frac{\partial(\Delta\mathbf{S})}{\partial(\Delta\boldsymbol{\varepsilon})} = 2G \left\{ \frac{\partial(\Delta\boldsymbol{\varepsilon}')}{\partial(\Delta\boldsymbol{\varepsilon})} - \frac{3}{2} \frac{\mathbf{S} - \mathbf{X}}{J_2} \otimes \frac{\partial(\Delta p^{\text{in}})}{\partial(\Delta\boldsymbol{\varepsilon})} \right\} \tag{31}$$

Replacing the term of $\partial(\Delta\mathbf{S})/\partial(\Delta\boldsymbol{\varepsilon})$ with the above equation, Equation (29) can be re-written as

$$\frac{\partial(\Delta p^{\text{in}})}{\partial(\Delta\boldsymbol{\varepsilon})} = 2G\frac{\partial F}{\partial \mathbf{S}} : \frac{\partial(\Delta\boldsymbol{\varepsilon}')}{\partial(\Delta\boldsymbol{\varepsilon})} \Bigg/ \left\{ \frac{1}{\Delta t} + 3G\frac{\partial F}{\partial \mathbf{S}} : \frac{\mathbf{S}-\mathbf{X}}{J_2} - \frac{\partial F}{\partial \mathbf{X}} : \frac{\partial(\Delta\mathbf{X})}{\partial(\Delta p^{\text{in}})} - \frac{\partial F}{\partial \lambda}\frac{\partial(\Delta\lambda)}{\partial(\Delta p^{\text{in}})} - \frac{\partial F}{\partial c}\frac{\partial(\Delta c)}{\partial(\Delta p^{\text{in}})} - \frac{\partial F}{\partial D}\frac{\partial(\Delta D)}{\partial(\Delta p^{\text{in}})} - \frac{\partial F}{\partial \mu}\frac{\partial(\Delta\mu)}{\partial(\Delta p^{\text{in}})} \right\} \tag{32}$$

where the 6×6 matrix form of $\partial(\Delta\boldsymbol{\varepsilon}')/\partial(\Delta\boldsymbol{\varepsilon})$ is derived as

$$\frac{\partial(\Delta\boldsymbol{\varepsilon}')}{\partial(\Delta\boldsymbol{\varepsilon})} = \begin{bmatrix} 2/3 & -1/3 & -1/3 & 0 & 0 & 0 \\ -1/3 & 2/3 & -1/3 & 0 & 0 & 0 \\ -1/3 & -1/3 & 2/3 & 0 & 0 & 0 \\ 0 & 0 & 0 & 1 & 0 & 0 \\ 0 & 0 & 0 & 0 & 1 & 0 \\ 0 & 0 & 0 & 0 & 0 & 1 \end{bmatrix} \tag{33}$$

Therefore, the damage-coupled instantaneous tangent stiffness matrix $\mathbf{J}$ can be determined with Equations (28) and (32).

4. NUMERICAL EXAMPLES

The proposed model was used to predict the tensile behaviour of a lap-joint specimen as depicted in Figure 1 with ABAQUS and the new constitutive subroutine for solder. There are 18 joints in the specimen. The dimensions of each joint are $1.778\times 1.778\times 0.254\ \text{mm}^3$ ($0.07\times 0.07\times 0.01\ \text{in}^3$). The specimen was used for monotonic tensile test under displacement control of 0.254×10^{-3} mm/s at room temperature (25°C). The values of Young's modulus and strength of copper are much higher than those of solder, so the portion of the specimen made of copper may be assumed as a rigid body. Therefore, only one joint is chosen for the FEA analysis due to similar geometry and boundary conditions experienced by all joints.

Several numerical tests were performed to check for mesh dependency. Different mesh refinements, including 2×7, 4×14, 8×28 and 16×56 elements, respectively, were chosen for the joint as shown in Figure 2. Two brick solid elements C3D8R (8-node linear, reduced integration with hourglass control) and C3D8 (8-node linear, full integration) were used. The numerical results were found to be almost the same for different combinations of

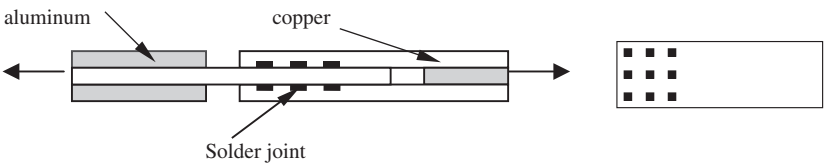

Figure 1. Lap-joints specimen (18 joints of $1.778\times 1.778\times 0.254\ \text{mm}^3$).

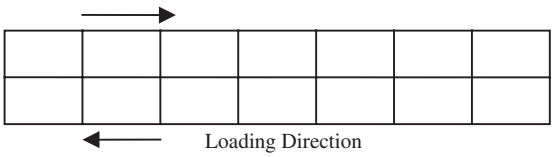

Figure 2. Coarse mesh with 2×7 elements.

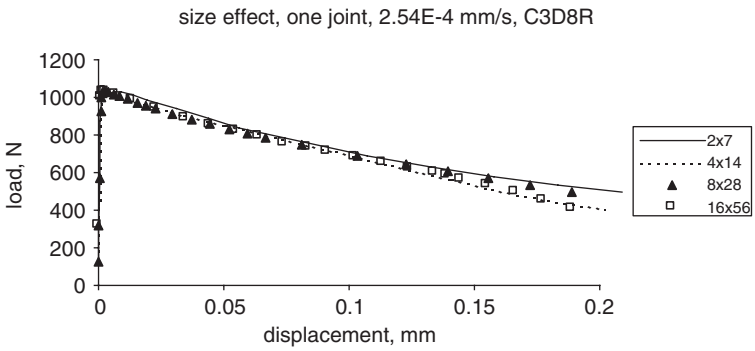

Figure 3. Effects of mesh refinement on predicted load vs displacement.

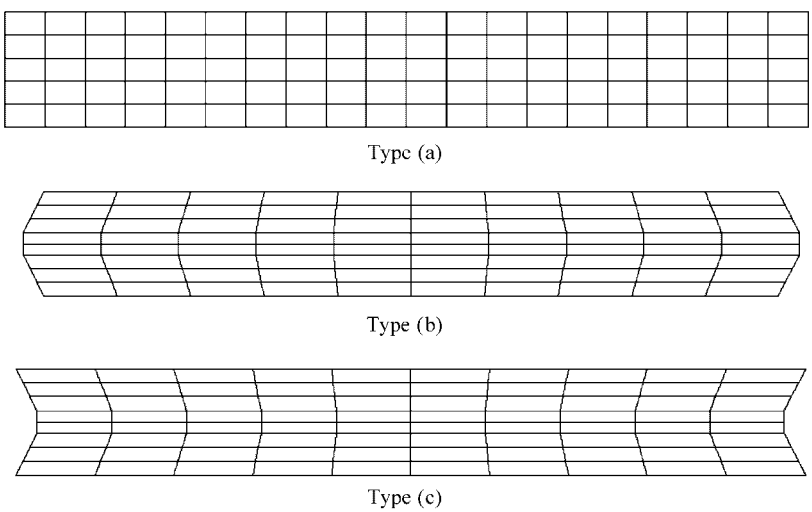

Figure 4. Finite element models of solder joints with 3 different geometries.

element sizes and types up to 50% load–drop. The calculated load–displacement curve along the loading direction is shown in Figure 3.

Three different types of solder joint configurations each containing the same cross-sectional area at the minimum section were examined as shown in Figure 4. The calculated load history curves for the three joint configurations are nearly the same as shown in Figure 5. Numerical

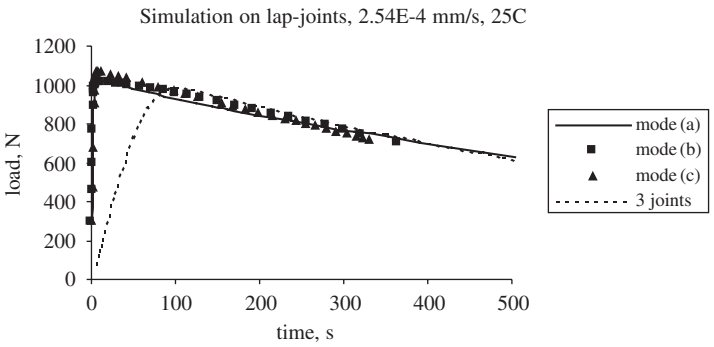

Figure 5. Load history curves.

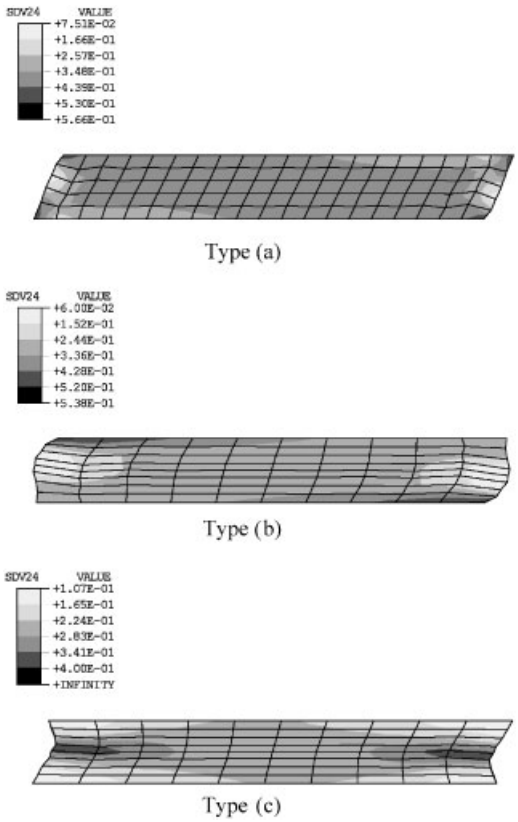

Figure 6. Damage distribution for models with different initial geometries.

studies on mesh dependency were also carried out for two irregular configurations (b) and (c) in Figure 4. Similar to the result shown in Figure 3 for regular configuration, no significant dependency was observed for these irregular shapes. It can be observed from Figure 6 that

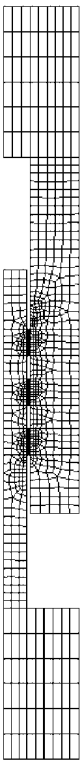

Figure 7. Finite element model of section through lap-joint specimen.

the corresponding damage distributions are however different. The maximum damage appears at the boundary for Types (a) and (b), revealing failure near the boundary, while Type (c) exhibits failure in the mid-layer of the section.

Figure 7 depicts the finite element discretization chosen for the lap-joint specimen as a plane strain, two-dimensional structure, assuming no variation of stress–strain distribution along the width direction. Hence only three solder joints are simulated. The portions of the specimen made of copper and aluminum alloy are simulated as linear-elastic materials. The discretization of the specimen consists of seven element layers through the solder joint in the width direction. Both the linear, full-integration (C3D8) and the reduced-integration (C3D8R) solid elements were employed. The load–drop curve is shown in Figure 5 together with three different one-joint simulations mentioned above. It can be readily observed from the figure that the maximum load for the three-joint simulation is lower than that of the single-joint simulations, although all the curves merge during softening. The predicted maximum loads from the simulations are summarized in Table III together with the measured result. It can be observed from the table that the numerical solution is slightly lower than the test result. The discrepancy in the prediction may be attributed in part to the two-dimensional simulations of the three-dimensional lap-joint specimen and to material parameters determined from the bulk material of 63Sn–37Pb. More detailed analyses will be carried out to examine the results of

Table III. Maximum load (N) with loading rate of 2.54×10^{-4} mm/s at 25°C.

Mode(a)	Mode(b)	Mode(c)	3 Joints	Test result
1025	1014	1068	988	1090

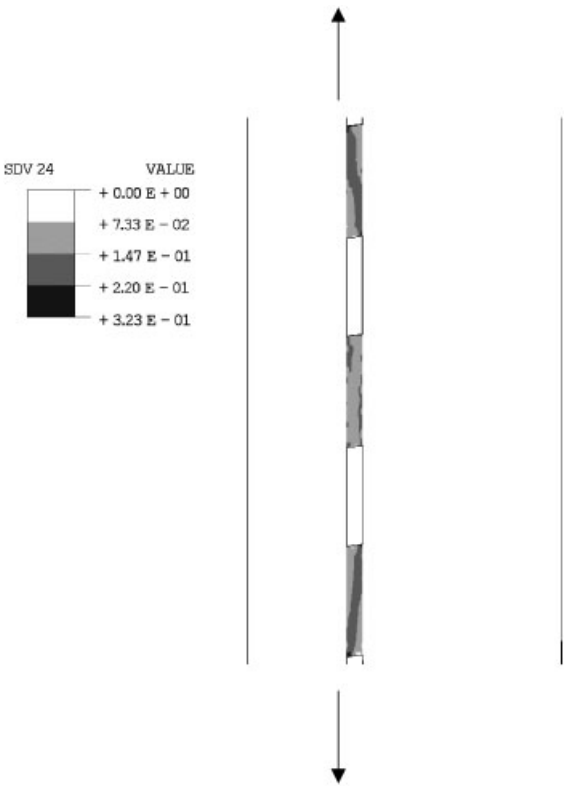

Figure 8. Damage distribution for lap-joint specimen.

three-dimensional simulations and the differences between the properties of the bulk solder material and the solder in joints.

The numerical simulation also reveals that the maximum damage in the middle joint is lower than other joints as shown in Figure 8. Therefore, those leading-edge joints with higher damage accumulation are expected to be the potential sites of failure.

5. CONCLUSIONS

A concept of damage surface is introduced in this study to differentiate the type of damage generated by different loading histories. This concept enables the formulation of a unified

damage evolution equation for finite element analysis under complex loading, including monotonic loading and cyclic loading. An investigation of mesh dependency of solder joint analyses with the proposed material model reveals that the mesh dependence is negligible before the damage accumulation reaches a critical value (or 50% load–drop). In addition to the load–drop curve of the lap-joint specimen, the model can be used to predict the potential failure location of joints from the simulated damage contours.

ACKNOWLEDGEMENTS

This work was supported by the United States Department of Energy under Contract DE-AC04-94AL85000. Sandia is a multiprogram laboratory operated by Sandia Corporation, a Lockheed Martin Company, for the United States Department of Energy.

REFERENCES

1. Busso EP, Kitano M, Kumazawa T. Modeling complex inelastic deformation processes in IC packages' solder joints. *Journal of Electronic Packaging* (ASME) 1994; **116**:6–15.
2. McDowell DL, Miller MP, Brooks DC. A unified creep-plasticity theory for solder alloys. *Fatigue of Electronic Materials*, *ASTM STP* 1994; **1153**:42–59.
3. Frear DR, Burchett SN, Neilsen MK, Stephens. Microstructurally based finite element simulation of solder joint behaviour. *Soldering and Surface Mount Technology* 1997; **2**:39–42.
4. Basaran C, Yan CY. A thermodynamic framework for damage mechanics of solder joints. *Journal of Electronic Packaging* (ASME) 1998; **120**:379–384.
5. Wei Y, Chow CL, Fang HE, Neilsen MK. Constitutive modeling of viscoplastic damage in solder material. *IUTAM Symposium on Creep in Structures*. Dordrecht: Kluwer, 2000; 131–140.
6. Chaboche JL, Cailletaud G. Integration methods for complex plastic constitutive equations. *Computer Methods in Applied Mechanics and Engineering* 1996; **133**:125–155.
7. Hartmann S, Luhrs G, Haupt P. An efficient stress algorithm with applications in viscoplasticity and plasticity. *International Journal for Numerical Methods in Engineering* 1997; **40**:991–1013.
8. Desai CS, Basaran C, Zhang W. Numerical algorithms and mesh dependence in the disturbed state concept. *International Journal for Numerical Methods in Engineering* 1997; **40**:3059–3083.
9. Qian Z, Liu S. Implementation of unified viscoplasticity with damage evolution and its application to electronic packaging. *Advances in Electronic Packaging* 1999; **26**(2):2099–2106.
10. Wei Y, Chow CL, Neilsen MK, Fang HE. Damage mechanics based fatigue life prediction for 63Sn–37Pb solder material. *ASME International Mechanical Engineering Congress and Exposition* 2000; **EEP-28**:161–165.
11. Wei Y, Chow CL, Fang HE, Neilsen MK. Characteristics of creep damage for 60Sn–40Pb solder material. *Journal of Electronic Packaging* (ASME) 2001; **123**:278–283.
12. Fu C, McDowell DL, Ume IC. A finite element procedure of a cyclic thermoviscoplasticity model for solder and copper interconnects. *Journal of Electronic Packaging* (ASME) 1998; **120**:24–34.
13. Vianco PT, Burchett SN, Neilsen MK, Rejent JA, Frear DR. Coarsening of the Sn–Pb solder microstructure in constitutive model based prediction of solder joint thermal mechanical fatigue. *Journal of Electronic Materials* 1999; **28**:1290–1298.
14. Hibbitt, Karlsson & Sorensen, Inc., Equilibrium and virtual work, *ABAQUS Theory Manual*, version 5.8, 1998; 1.5.1.

